Journal of Physics: Condensed Matter

PAPER

Cationic distribution and spin canting in $CoFe_2O_4$ nanoparticles

To cite this article: D Peddis *et al* 2011 *J. Phys.: Condens. Matter* **23** 426004

J. Phys.: Condens. Matter **23** (2011) 426004 (8pp) doi:10.1088/0953-8984/23/42/426004

Cationic distribution and spin canting in $CoFe_2O_4$ nanoparticles

D Peddis[1,2], N Yaacoub[3], M Ferretti[4,5], A Martinelli[5], G Piccaluga[1], A Musinu[1], C Cannas[1], G Navarra[1], J M Greneche[3] and D Fiorani[2]

[1] Dipartimento di Scienze Chimiche, Cittadella Universitaria di Monserrato, bivio per Sestu, 09042, Monserrato, Italy
[2] ISM-CNR, Area ROMA1, Via Salaria km 29.500, 00016 Roma, Italy
[3] Université du Maine, Laboratoire de Physique de l'Etat Condensé UMR CNRS 6087, Le Mans, France
[4] Dipartimento di Chimica e Chimica Industriale, Università di Genova, Via Dodecaneso 31, I-16146 Genova, Italy
[5] SPIN-CNR, C.so Perrone 24, I-16152 Genova, Italy

Received 15 July 2011, in final form 5 September 2011
Published 7 October 2011
Online at stacks.iop.org/JPhysCM/23/426004

Abstract
$CoFe_2O_4$ nanoparticles ($\langle D_{NPD}\rangle \sim 6$ nm), prepared by a thermal decomposition technique, have been investigated through the combined use of dc magnetization measurements, neutron diffraction, and ^{57}Fe Mössbauer spectrometry under high applied magnetic field. Despite the small particle size, the value of saturation magnetization at 300 K ($M_s \cong 70$ A m^2 kg^{-1}) and at 5 K ($M_s \cong 100$ A m^2 kg^{-1}) are rather close to the bulk values, making the samples prepared with this method attractive for biomedical applications. Neutron diffraction measurements indicate the typical ferrimagnetic structure of the ferrites, showing an inversion degree ($\gamma_{NPD} = 0.74$) that is in very good agreement with cationic distribution established from low temperature (10 K) Mössbauer measurements in high magnetic field ($\gamma_{moss} = 0.76$). In addition, the in-field Mössbauer spectrum shows the presence of a non-collinear spin structure in both A and B sublattices. The results allow us to explain the high value of saturation magnetization and provide a better insight into the complex interplay between cationic distribution and magnetic disorder in ferrimagnetic nanoparticles.

(Some figures in this article are in colour only in the electronic version)

1. Introduction

Magnetic nanomaterials are the subject of continuing interest both because of their wide fields of applications (e.g. magnetic recording, electronics, biomedicine, catalysis, etc) [1–3] and for their unique physical properties, greatly differing from those of their parent bulk materials [4]. Among the relevant features of the size reduction of magnetic particles, the presence of a non-collinear spin structure (spin canting) deserves special attention, as it determines strong modifications in the magnetic properties. For this reason spin canting has been intensively studied for more than 30 years. Several studies on ferrimagnetic iron oxides with spinel structure (γ-Fe_2O_3 and Fe_3O_4) showed that even in a very large magnetic field some atomic moments did not align with the external field. This feature was ascribed to magnetic disorder at the particle surface due to competing interactions between sublattices [5–7]. This hypothesis was also confirmed by polarized neutron scattering [8] and ^{57}Fe Mössbauer experiments [9] in Co and Ni ferrites, respectively. The symmetry breaking induces changes in the topology of the superficial magnetic moments and consequently in exchange integrals (through superexchange angles and/or distances between moments) thus leading to surface anisotropy [4, 10].

Among the nanoscale materials, magnetic nanoparticles of ferrites ($Me^{II}Fe_2O_4$; $Me^{II} = Fe^{2+}$, Ni^{2+}, Co^{2+}, etc) with spinel structure have generated much interest, not only for their technological application, but also because the rich crystal chemistry of spinels offers excellent opportunities for fine tuning of the magnetic properties [11, 12]. The spinel ferrite has a face-centred cubic (fcc) structure in which the oxygen atoms are cubic close-packed. The structure contains two interstitial sites, occupied by metal cations, with tetrahedral, A-site, and octahedral, B-site, oxygen

coordination, resulting in a different local symmetry. In general, the cationic distribution in octahedral and tetrahedral sites may be quantified by the inversion degree (γ), which can be defined as the fraction of divalent ions in the octahedral sites [13]. The net magnetization can be considered proportional to the difference between A and B sublattice magnetization, so that the saturation magnetization depends on the cationic distribution. Also the magnetic anisotropy is related to inversion degree because single ion anisotropy of the divalent ions depends on interstitial site.

Thus, the magnetic properties of ferrite nanoparticles with spinel structure are due to a complex interplay of several effects, where cation distribution and spin canting are fundamental factors. Neutron diffraction and ^{57}Fe Mössbauer studies have provided evidence that spin canting can be either restricted to a single magnetic sublattice [9] or extended to both cationic sites [14] and this leads us to believe that spin canting is strictly connected with the cation distribution. In this general framework, the inter-dependence between inversion degree and magnetic disorder and their influence on the magnetic properties of the materials represent one of the most important topics in the physical chemistry study of the nanostructured spinel ferrites.

In order to gain a better insight into the effect of the complex interplay between cation distribution and spin canting on magnetic properties, a careful study of crystalline and magnetic structure of $CoFe_2O_4$ nanoparticles is presented. The powder sample, prepared by a thermal decomposition method, shows very interesting magnetic properties (e.g. higher saturation magnetization with respect to the bulk material [15]). We report a comparative study using neutron powder diffraction (NPD) and ^{57}Fe Mössbauer spectrometry under high magnetic field. Because of the marked difference in the nuclear scattering amplitude of the cations, NPD allows us to obtain very precise information about crystalline structure. In-field ^{57}Fe Mössbauer spectrometry is a powerful tool to analyse carefully the local magnetic behaviour of Fe species, getting information about magnetic structure of the nanoparticles.

2. Experimental details

The details of the synthesis procedure have been reported elsewhere [15]. Aqueous solutions of $Fe(NO_3)_3{*}9H_2O$ (Aldrich, 98%), $Co(NO_3)_2{*}6H_2O$ (Aldrich, 98%) and citric acid (Aldrich, 99.9%) were mixed together in a Pyrex beaker with 1:1 molar ratio of metals to citric acid; the pH of the sol thus obtained was <1. The sol was allowed to gel on a hot plate, maintaining the solution temperature at 80–90 °C. A sudden increase of the temperature ($T > 200$ °C) induced a slow reaction that leads after about 10 min to a grey powder [15].

NPD analysis was carried out at the Institute Laue Langevin (Grenoble, France). High resolution NPD patterns were collected at 300 K using the D1A diffractometer ($\lambda = 1.91$ Å). Rietveld refinement of NPD data was carried out using the program Fullprof [16]; by means of an NAC standard an instrumental resolution file was obtained and applied during refinements in order to detect micro-structural contributions to the NPD peak shape. The diffraction lines were modelled by a Thompson–Cox–Hastings pseudo-Voigt convoluted with axial divergence asymmetry function and the background by a fifth-order polynomial. The following parameters were refined: the overall scale factor; the background (five parameters of the fifth-order polynomial); 2θ-zero; the unit cell parameters; the specimen displacement; the reflection-profile asymmetry; the Wyckoff positions not constrained by symmetry; the isotropic thermal parameters B; the Lorentzian isotropic strain and size parameters; the occupancies at the tetrahedral and octahedral sites.

dc magnetization measurements were performed by a commercial Quantum Design superconducting quantum interference device (SQUID) magnetometer ($H_{max} = 5$ T). The powdered sample was immobilized in an epoxy resin in order to prevent any movement of the nanoparticles during the measurements.

A ^{57}Fe Mössbauer spectrum was recorded using a ^{57}Co/Rh γ-ray source mounted on an electromagnetic transducer with a triangular velocity form. It was obtained at 10 K in an 8 T field oriented parallel to the γ-beam. For the analysis of Mössbauer spectra the program 'Mosfit' has been used. The hyperfine structure was modelled by a least-squares fitting procedure involving Zeeman sextets composed of Lorentzian lines. To describe the broadening of lines, several magnetic subcomponents have been considered where isomer shift, quadrupolar shift, linewidth and effective field values were free during the refinement and the intensities of intermediate lines (2, 5) as well; the ratio of intensities of external/internal lines being systematically equal to 3. The isomer shift (IS) values were referred to α-Fe at 300 K. The samples consist of a thin layer of about 40 mg of the powdered compound located in a sample holder.

3. Results and discussion

A structural, morphological, textural, and magnetic investigation of the sample is given elsewhere [15]. Some published magnetic results will be recalled in order to build a framework to discuss the correlation between inversion degree and spin canting. The temperature dependence of magnetization, measured by zero-field cooled (ZFC) and field cooled (FC) protocols, suggests the presence of a non-negligible fraction of nanoparticles still in the magnetic blocked state at room temperature. Indeed, ZFC and FC magnetizations do not overlap in the temperature range 5–300 K. The FC curve exhibits a temperature independent behaviour in the range 200–5 K, thus suggesting the presence of interparticle interactions [15]. Virgin magnetization curves recorded at 300 K (full symbols) and at 5 K (empty symbols) are reported in figure 1. At 5 K the curve is S-shaped, as observed in disordered assemblies of nanoparticles with competing interparticle interactions (spin-glass-like state) [17]. Both the lack of magnetic saturation (i.e. increase of slope at high field) and the high coercivity ($H_c \cong 1.6$ T) [15] indicate high magnetic anisotropy [18, 19].

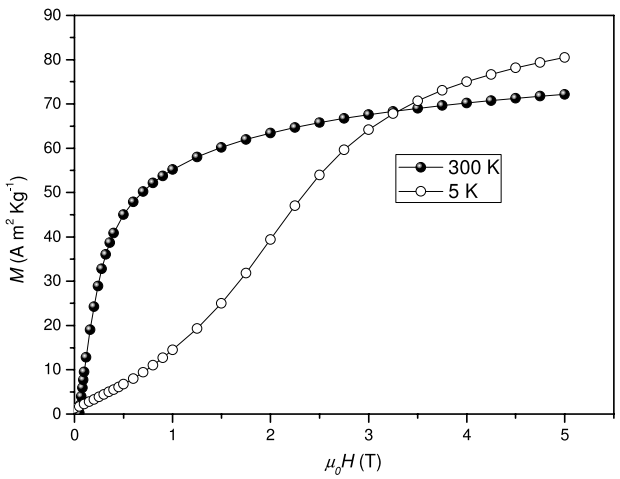

Figure 1. Virgin magnetization curves at 300 K (full symbols) and 5 K (empty symbols).

The saturation magnetization (M_s) value was estimated by fitting the high-field part of the magnetization curves using the relation [20]:

$$M = M_s \times \left(1 - \frac{a}{H} - \frac{b}{H^2}\right) \quad (1)$$

where H is the field strength, and a and b two parameters determined by the fitting procedure. The values of the magnetic moment × chemical formula ($\mu_{C.F.}$) of 4.17 μ_B and 3.41 μ_B are obtained at 5 and 300 K, respectively.

The crystalline and magnetic structures of the samples were investigated by NPD at 300 K. Rietveld refinement of the NPD pattern (figure 2) indicates only the presence of the $CoFe_2O_4$ phase crystallized in the $Fd\bar{3}m$ space group with mean particle size around 6 nm. The marked difference in nuclear scattering amplitude between cobalt and iron ions allows us to obtain the cation distribution (table 1), with an inversion degree of $\gamma = 0.74$. Structural values obtained by Rietveld refinement are in very good agreement with expected values for nanoscale $CoFe_2O_4$ (table 1) [11, 12].

Nanoparticles display the typical ferrimagnetic structure of the inverse ferrites, with the magnetization of the B sublattice oppositely directed to that of the A sublattice; spins are aligned along one of the cubic axes. The refined magnetic moments at the A and B sublattices are lower with respect to the values reported in the literature for $CoFe_2O_4$ nanoparticles with similar particle size and cationic distribution [11]. This leads us to believe that some non-collinear spin components coexist with the ordered spins. At room temperature the canted spins are randomly oriented and they do not contribute to the Bragg peaks, being responsible for the reduced ordered moments [21].

Mössbauer spectra of ferrites in large applied fields do allow a more reliable distinction between A- and B-site components than the zero-field spectra, because the applied field is usually added to the A-site hyperfine field and subtracted from the B-site hyperfine field. Therefore, there is less overlap between the two components in the high-field spectra. Furthermore, in the presence of an external magnetic field parallel to the γ-ray direction, the relative areas of the six lines give information about the degree of alignment of the magnetization with the applied field.

Figure 3 illustrates the spectrum obtained at 10 K under a magnetic field of 8 T applied parallel to the γ-beam. The spectrum is consistent with a ferrimagnetic structure without any superparamagnetic relaxation states. Indeed, the Mössbauer spectrum recorded at 77 K without external field (not reported here) consists of a pure magnetic sextet composed of asymmetrical lines: it is concluded at 77 K and below that the nanoparticles are in the blocked magnetic state, thus excluding superparamagnetic relaxation phenomena. In addition, the refinement of the in-field spectrum allows us to attribute clearly the two magnetic components to the Fe^{3+} in tetrahedral and octahedral sites, according to the values of the isomer shift. Then, an accurate value of the atomic Fe_A^{3+}/Fe_B^{3+} population ratio has been obtained (table 2). In addition, one can note that the hyperfine structure does not evidence at all the presence of Fe^{2+} ions. The area ratio $Fe_{A,B}^{3+}/Fe_{total}^{3+}$ of the A and B subspectra is typical of Co-ferrite with partially inverted spinel structure. The

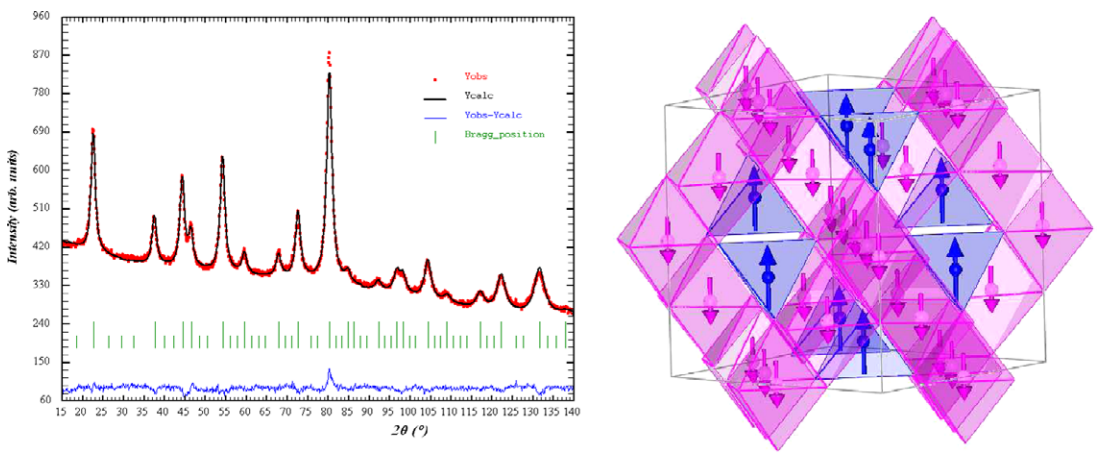

Figure 2. Left part: neutron diffraction pattern (symbols) and Rietveld refinement (line). Right part: diagram of magnetic structure.

Table 1. Structural data and sublattice magnetic moments obtained from Rietveld refinement of NPD data at 300 K; the samples crystallize in the $Fd\bar{3}m$ space group (origin choice 2; A site: 8a; B site: 16d; O at 32e).

Rietveld refinement							
Cell size (Å)	O coordinate (x)	$\langle D \rangle$ (nm)	μ_{Td} (μ_B)	μ_{Oh} (μ_B)	R-Bragg (%)	R-factor (%)	R-magnetic (%)
8.3777(4)	0.2564(1)	6.0	4.05(7)	2.95(5)	3.46	1.65	3.00
Cationic distribution				$(Fe_{0.73}Co_{0.27})[Fe_{0.63}Co_{0.37}]_2O_4$			

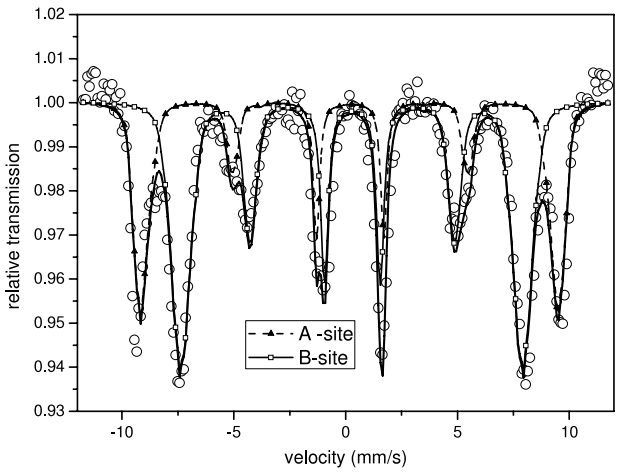

Figure 3. ^{57}Fe Mössbauer spectrum obtained at 10 K in 8 T magnetic field applied parallel to the γ-beam. Note that the second and fifth lines have non-zero intensity, showing that the magnetic structure is not collinear.

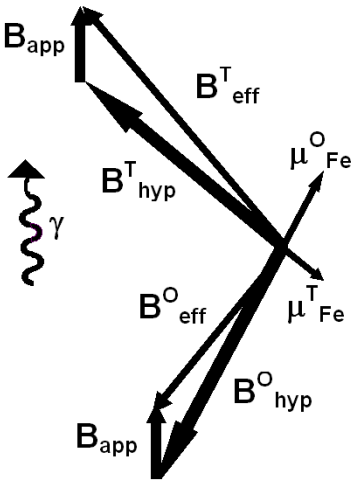

Figure 4. Schematic representation of the vector diagram of the hyperfine fields (B_{hyp}) of the ions Fe^{3+} in sites A and B under an applied magnetic field (B_{app}).

Table 2. In-field Mössbauer fitted parameters of the $CoFe_2O_4$: isomer shift (δ), quadruple shift (2ε), canting angle (θ), and the relative fraction of the Fe^{3+} located in A and B sites ($Fe^{3+}_{A,B}/Fe^{3+}_{total}$).

Mössbauer hyperfine parameters of the Co-ferrite				
	$\langle\delta\rangle$ (mm s^{-1}) ±0.01	$\langle 2\varepsilon\rangle$ (mm s^{-1}) ±0.01	$\langle\theta\rangle$ (deg) ±10	$Fe^{3+}_{A,B}/Fe^{3+}_{total}$ ± 0.01
Fe^{3+}_A	0.36	−0.04	41	0.38
Fe^{3+}_B	0.47	−0.03	36	0.62

cation distribution for stoichiometric $CoFe_2O_4$ can be given as $(Fe_{0.76}Co_{0.24})[Fe_{0.62}Co_{0.38}]_2O_4$, with $\gamma_{Moss} = 0.76$. It should be emphasized that the inversion degree obtained by in-field Mössbauer investigation is in good agreement with that estimated from NPD analysis ($\gamma_{NPD} = 0.74$), within the experimental error of the two techniques.

The modelling of the in-field Mössbauer spectrum allows us also a direct estimation of both the effective field (B_{eff}) and the angle (θ) of the two types of sites, and then their respective hyperfine field B_{hyp} can be calculated according to the relation:

$$B^2_{hyp} = B^2_{eff} + B^2_{app} - 2B_{eff}B_{app}\cos\theta \qquad (2)$$

where B_{eff} is the vectorial sum of the B_{hyp} and the applied field B_{app}, and θ corresponds to the angle defined by the direction of the effective field for both tetrahedral and octahedral iron components and the γ-beam direction. Figure 4 is a representation of the vector diagram of the B_{hyp} (or B_{eff}) of the ions Fe^{3+} in the A and B sites under a B_{app}. Note that the in-field spectrum (figure 3) shows that the second and fifth lines have a non-zero intensity. Usually, when these peaks are distinctly observed, they evidence a canted structure for Fe^{3+} magnetic moments with respect to the applied field (non-collinear magnetic structure) [4, 6, 22]. For a thin absorber the relative area of the six lines is given by 3: p:1:1: p:3, where [22, 23]:

$$p = \frac{4\sin^2\theta}{1+\cos^2\theta}. \qquad (3)$$

In the case of a microcrystalline chemically ordered ferrite, the lines of A and B subspectra are not broadened, thus allowing the values of B_{eff}(A) and B_{eff}(B) and those of θ(A) and θ(B) to be practically estimated. In contrast, asymmetrical broadening of lines occurs when the structure is chemically disordered or influenced by surface or grain boundaries originating from finite size effects in the case of nanostructured systems [24, 25]. In this case the fitting model becomes quite complex, because it does involve magnetic effective field distributions ($P(B_{eff})^{A,B}$) correlated to canting angle distribution ($P(\theta)^{A,B}$). It is thus necessary to establish first carefully such a joint distribution taking into account the physical origin and then to check whether the estimated $P(B_{hyp})$ is able to well describe the zero-field spectrum. $P(B_{eff})^{A,B}$ and $P(\theta)^{A,B}$ are illustrated in figure 5 (upper part) in the case of present Co-ferrite nanoparticles

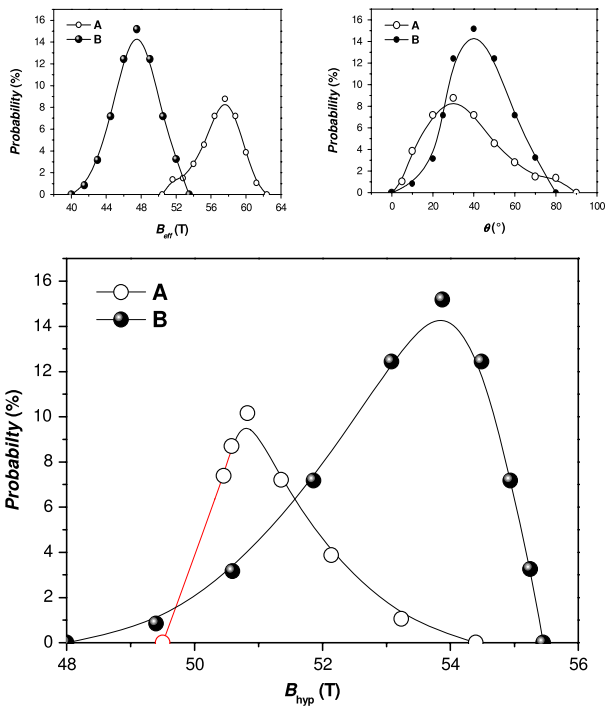

Figure 5. Left-upper part: distribution of the effective magnetic field. Right-upper part: distribution of canting angles, $P(\theta)$, correlated with $P(B_{hf})$, obtained by the fitting procedure. Lower part: distribution of the hyperfine magnetic field $P(B_{hyp})$ observed for both sites A and B, obtained by equation (2).

together with $P(B_{hyp})^{A,B}$ (figure 5, lower part) estimated from previous ones. As cationic inversion is clearly evidenced from the proportions of Fe^{3+} ions located in tetrahedral and octahedral sites, both Co^{2+} and Fe^{3+} cations occupy simultaneously the A and B sites. The number of different B (A)-sites fields and their relative intensity could be correlated with the probability of having a certain number of Co^{2+} A (B)-sites surrounding a given Fe^{3+} B (A)-site ions. The correlation between B_{hf} and canting angle allows us to relate $P(B_{hf})$ and $P(\theta)$ to the cation distribution (inversion degree, Fe^{3+} ions in B (A)-sites with nearest-neighbours Co^{2+} A (B)-site ions) and to surface effects. The average angle values for Fe^{3+} in tetrahedral and octahedral sites are thus about 41°and 36°, respectively. The broadening of Mössbauer lines, i.e. hyperfine field distributions, suggests unambiguously different atomic neighbouring of Fe sites. It has been established that the hyperfine field at the octahedral Fe site decreases by about 0.6–1.0 T per Co nearest neighbour located in the tetrahedral site [26]. As illustrated in figure 5, the corresponding hyperfine field distribution ranges from 55.5 and 49.5 T, in agreement with Fe with six A-Fe up to six A-Co first neighbours. By correlation to the effective field distribution, one easily concludes that the smallest effective field values have to be associated to Fe moments which are aligned with the external field to give rise to the lowest hyperfine field value (similarly the increasing effective field values have to be associated to canted Fe^{3+} magnetic moments, giving rise to the highest hyperfine field values). This description is confirmed by comparing hyperfine and effective field distributions characteristic of tetrahedral Fe^{3+} ions, but the effects are less important than in the case of octahedral Fe sites. Consequently, such features suggest a chemical inhomogeneity: a Co-enriched nanoparticle core and Fe-enriched and magnetically canted shell, giving rise to a progressive cationic gradient within the nanoparticle. It is relevant to underline that this description is more complete than that established from neutron diffraction which is concerned with the mean values. Finally it is important to emphasize that some recent Mössbauer studies on monodisperse $CoFe_2O_4$ nanoparticles, synthesized by forced hydrolysis in polyol, with different diameters ranging from 2.4 to 6.2 nm, gave rise to rather narrow Mössbauer lines, suggesting less cationic disorder [27]. Such differences can originate from the synthesis process used to prepare the present sample, involving a relatively fast thermal decomposition reaction [15].

3.1. Correlation between spin canting and cationic distribution

The spin canting in ferrimagnetic non-interacting nanoparticles is most likely attributed to different origins: (1) the cationic inversion due to chemical disorder which modifies superexchange interactions; (2) the surface effect due to the symmetry breaking originating broken exchange bonds at the external layer of the nanoparticles (nearest-neighbours at the surface different from the bulk ones). Both these effects give rise to magnetic topological frustration and consequently a spin canting occurs [28, 29]. In addition, it is important to emphasize the local anisotropy, which is strong in the case of Fe^{2+}, Ni^{2+} and especially Co^{2+} ions, contrary to that of Fe^{3+} and Mn^{2+}.

The spin canting may be explained, in ferrimagnetic structures, in terms of the Yafet–Kittel triangular arrangement due to the magnetic frustration resulting from the competition between A–B and B–B exchange interactions. Indeed, generally speaking, the main features of the spin structure may be understood on the basis of the expression for the magnetic energy of an ion located, for example, in the B sites [30, 31]:

$$E_B = E_a + (g\mu_B \vec{S}_{B_h} \cdot \vec{B}_{app}) - S_{B_h} \cdot \left(\sum_i J_{A1} S_{Ai} + \sum_j J_{B1} S_{BJ} + \cdots \right) \quad (4)$$

where E_a represents the magnetic anisotropy energy and the second term the interaction of the spin S_B with an applied field. In the first approximation, we consider only the next neighbouring magnetic ions: in the third term J_{A1} and J_{B1} represent exchange coupling constants of spin S_B with the spins located in the next neighbouring A and B site respectively [32]. For the Fe^{3+} ions the contribution of the anisotropy energy to the magnetic energy is expected to be small compared to the exchange energy [33], and the spin structure can be considered related mainly to the exchange coupling energy. On the other hand, for Co^{2+} ions the anisotropy energy is quite high [22] and this determines a strong increase of magnetic energy. Then, the

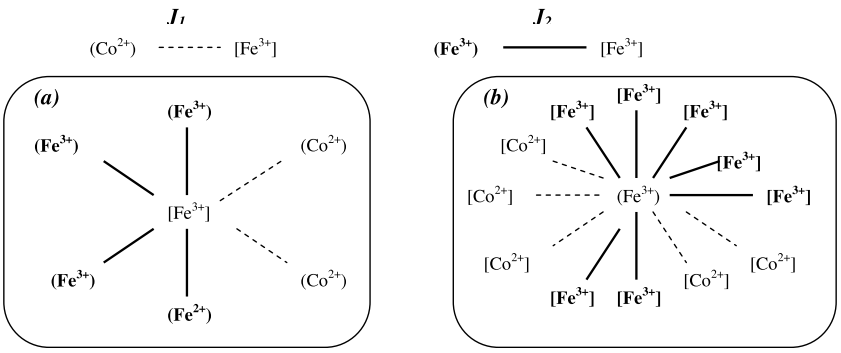

Figure 6. Schematic representation of the magnetic environment of iron atoms located in A (a) and B (b) sites.

high single ion anisotropy of Co^{2+} indicates that the canting involves mainly Fe^{3+} ions, as already observed in molecular compounds [18, 34].

In a spinel ferrite structure each tetrahedral Fe^{3+} ion is surrounded by 12 octahedral ions, while an octahedral Fe^{3+} ion has only six tetrahedral nearest-neighbours [26]. Starting from the cationic distribution obtained by the in-field Mössbauer spectrum and NPD pattern, we can assume that in our nanoparticles each B–Fe^{3+} has on average two A–Co^{2+} and four A–Fe^{3+} (figure 6(a)) neighbours. On the other hand an A–Fe^{3+} atoms is surrounded on average by seven B–Fe^{3+} and five B–Co^{2+} (figure 6(b)). Calculation based on molecular-field theory indicates that the superexchange interactions [Fe^{3+}]–O^{2-}–(Co^{2+}), $J_1 = 13.7$ K, are weaker than [Fe^{3+}]–O^{2-}–(Fe^{3+}), $J_2 = 20.1$ K [26]. Then, Fe atoms located in the octahedral site are surrounded by ∼67% of iron atoms in tetrahedral site, while iron atoms on A sites have as next neighbouring ∼59% of iron atoms in B sites (figure 6). Then, Fe^{3+} with octahedral and tetrahedral symmetry feel a similar total superexchange strength. Keeping in mind that J_{AB} interactions are predominant with respect to J_{AA} and J_{BB} [31], these arguments qualitatively explain why the canting in this sample extends to both A and B sites. It is worth noting that this model is in good agreement with recent published data on $CoFe_2O_4$ nanoparticles prepared by a similar synthesis method [18]. In that case the Mössbauer spectrum under high magnetic field showed a magnetic structure where Fe^{3+} ions located in the B site are surrounded by ∼16% of iron atoms in the tetrahedral site, while iron atoms in A sites have as near neighbouring ∼84% of iron atoms in B sites. Thus, iron atoms located in the interstitial site with a tetrahedral symmetry feel a total superexchange strength which is definitely higher than that felt by the iron atoms located in an octahedral site. This explains why in that sample the canting was observed to be extended only to B sites.

3.2. Magnetic structure and saturation magnetization

One of the most controversial issues in the physical chemistry of the ferrimagnetic nanoparticles is the reduction of saturation magnetization with the particle size. In many studies on ferrimagnetic nanoparticles a reduction has been observed and attributed to spin canting that yields magnetic disorder at the particle surface [5, 7]. On the other hand, a steep rise in saturation magnetization at low temperature has been observed in ferrimagnetic nanoparticles and was explained by the freezing of surface spins [35–37]. The effect of magnetic disorder on saturation magnetization can be explained by the interplay between spin canting and inversion degree.

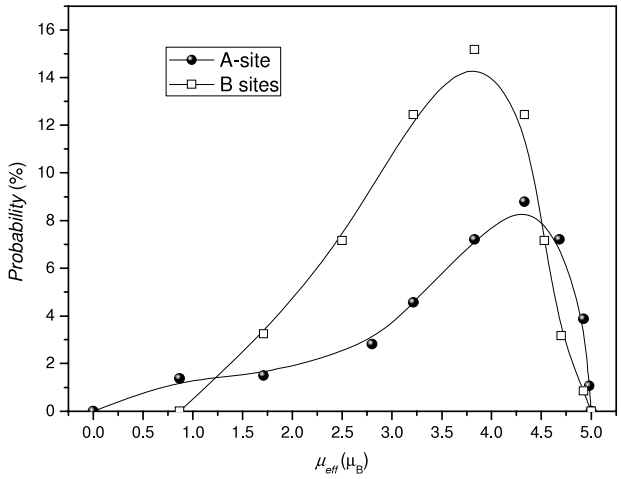

Figure 7. Distribution of effective magnetic moments (μ_{eff}) of iron atoms in A (full circles) and B (empty squares) sites.

Assuming that $Fe^{3+}$and Co^{2+} have a magnetic moment of 5 μ_B and 3 μ_B [38], respectively, and considering the canting angles it is possible to calculate the effective magnetic moment of each iron atom:

$$M_{eff} = M_{atomic} \times \cos\theta. \quad (5)$$

Using equation (5) and the distribution of canting angle extracted by in-field Mössbauer spectra it is possible to obtain the distribution of effective iron magnetic moments for each sublattice (figure 7), giving an indication of the influence of spin canting on magnetic moment.

The magnetic structure as described by Mössbauer spectrometry allows us to estimate the values of 2.32 μ_B and 3.44 μ_B for A and B sublattice mean magnetic moments. They correspond to $\mu_{C.F.}$ 4.56 μ_B, slightly higher (8.5%) than the value obtained by magnetization measurements (4.17 μ_B).

This small difference can be attributed to experimental error and/or to a weak canting of cobalt magnetic moments. Although we have a quite high spin canting, an increase of the $\mu_{C.F.}$ with respect to bulk materials (3.4–3.9 μ_B) is observed and this can be ascribed to a decrease of inversion degree ($\gamma_{bulk} = 0.82$). It is worth underlining that when canted spins are localized in the B sublattice, a stronger increase of $\mu_{C.F.}$ is observed [18].

4. Conclusions

By the combined use of dc magnetization measurements, neutron diffraction and in-field ^{57}Fe Mössbauer spectrometry, the correlation between magnetic properties and the magnetic structure of $CoFe_2O_4$ nanoparticles has been investigated. Neutron diffraction measurement indicates the typical ferrimagnetic structure of the inverse ferrites, showing an inversion degree of 0.74. This value is confirmed by the in-field Mössbauer spectrum ($\gamma_{moss} = 0.76$) that shows also the presence of a non-collinear spin structure in both A and B sublattices. Through these data a careful description of the magnetic structure of the nanoparticles is given and it allows us to have a better insight into the correlation between spin canting and cationic distribution. The results allow us to account quantitatively for the high value of saturation magnetization shown by this sample.

Acknowledgment

D Peddis was granted an award by RAS (Regione Sardegna—Centro regionale di Programmazione) co-founded by PO Sardegna FSE 2007–13 sulla L.R.7/2007 'Promozione della ricerca scientifica e dell'innovazione tecnologica in Sardegna.'

References

[1] Sun S 2006 Recent advances in chemical synthesis, self-assembly and applications of FePt nanoparticles *Adv. Mater.* **18** 393–403
[2] Suber L and Peddis D 2010 Approaches to synthesis and characterization of spherical and anisometric metal oxide magnetic nanomaterials *Magnetic Nanomaterials* vol 4 (New York: Wiley)
[3] Tartaj P, Del Puerto Morales M, Veintemillas-Verdaguer S, Gonzales Carreno T and Serna C J 2003 The preparation of magnetic nanoparticles for applications in biomedicine *J. Phys. D: Appl. Phys.* **36** R182–97
[4] Tronc E, Prené P, Jolivet J P, Dormann J L and Grenèche J M 1997 Spin canting in γ-Fe_2O_3 *Hyperfine Interact.* **112** 97–100
[5] Martínez B, Obradors X, Balcells L, Rouanet A and Monty C 1998 Low temperature surface spin-glass transition in gamma g-Fe_2O_3 nanoparticles *Phys. Rev. Lett.* **80** 181–4
[6] Coey J M D 1971 Noncollinear spin arrangement in ultrafine ferrimagnetic crystallites *Phys. Rev. Lett.* **27** 1140
[7] Lima J E, Brandl A L, Arelaro A D and Goya G F 2006 Spin disorder and magnetic anisotropy in Fe_3O_4 nanoparticles *J. Appl. Phys.* **99** 083908
[8] Lin D, Nunes A C, Majkrzak C F and Berkowitz A E 1995 Polarized neutron study of the magnetization density distribution within a $CoFe_2O_4$ colloidal particle II *J. Magn. Magn. Mater.* **145** 343–8
[9] Alves C R, Aquino R, Depeyrot J, Cotta T A P, Sousa M H, Tourinho F A, Rechenberg H R and Goya G F 2006 Surface spin freezing of ferrite nanoparticles evidenced by magnetization measurements *J. Appl. Phys.* **99** 08M905
[10] Tronc E *et al* 2003 Surface effects in noninteracting and interacting γ-Fe_2O_3 nanoparticles *J. Magn. Magn. Mater.* **262** 6–14
[11] Liu C, Zou B, Rondinone A J and Zhang Z J 2000 Chemical control of superparamagnetic properties of magnesium and cobalt spinel ferrite nanoparticles through atomic level magnetic couplings *J. Am. Chem. Soc.* **122** 6263–7
[12] Liu C, Rondinone A J and Zhang Z J 2000 Synthesis of magnetic spinel ferrite $CoFe_2O_4$ nanoparticles from ferric salt and characterization of the size-dependent superparamagnetic properties *Pure Appl. Chem.* **72** 37–45
[13] West A R 1984 *Solid State Chemistry and its Applications* (New York: Wiley)
[14] Oliver S A, Hamdeh H H and Ho J C 1999 Localized spin canting in partially inverted $ZnFe_2O_4$ fine powders *Phys. Rev.* B **60** 3400
[15] Cannas C, Falqui A, Musinu A, Peddis D and Piccaluga G 2006 $CoFe_2O_4$ nanocrystalline powders prepared by citrate–gel methods: synthesis, structure and magnetic properties *J. Nanopart. Res.* **8** 255–67
[16] Rodríguez-Carvajal J 1993 Recent advances in magnetic structure determination by neutron powder diffraction *Physica* B **192** 55–69
[17] Fiorani D, Del Bianco L and Testa A M 2006 Glassy dynamics in an exchange bias nanogranular system: Fe/FeO_x *J. Magn. Magn. Mater.* **300** 179–84
[18] Peddis D, Cannas C, Piccaluga G, Agostinelli E and Fiorani D 2010 Spin-glass-like freezing and enhanced magnetization in ultra-small $CoFe_2O_4$ nanoparticles *Nanotechnology* **21** 125705
[19] Kodama R H, Berkowitz A E, McNiff J E J and Foner S 1996 Surface spin disorder in $NiFe_2O_4$ nanoparticles *Phys. Rev. Lett.* **77** 394–7
[20] Morrish A H 1965 *The Physical Principles of Magnetism* (New York: Wiley)
[21] Yunus S M, Yamauchi H, Zakaria A K M, Igawa N, Hoshikawa A and Ishii Y 2007 Magnetic structural characterization of Mg–Co–Cr ferrite by neutron diffraction *J. Magn. Magn. Mater.* **310** 2722–4
[22] Cannas C, Musinu A, Piccaluga G, Fiorani D, Peddis D, Rasmussen H K and Mørup S 2006 Magnetic properties of cobalt ferrite–silica nanocomposites prepared by a sol–gel autocombustion technique *J. Chem. Phys.* **125** 164714
[23] Helgason O, Greneche J M, Berry F J, Mørup S and Mosselmans F 2001 Tin- and titanium-doped γ-Fe_2O_3 (maghemite) *J. Phys.: Condens. Matter* **13** 10785–97
[24] Hansen M F, Koch C B and Mørup S 2000 Magnetic dynamics of weakly and strongly interacting hematite nanoparticles *Phys. Rev.* B **62** 1124
[25] Morales M P, Serna C J, Bodker F and Morup S 1997 Spin canting due to structural disorder in maghemite *J. Phys.: Condens. Matter* **9** 5461
[26] Sawatzky G A, Van Der Woude F and Morrish A H 1969 Mössbauer study of several ferrimagnetic spinels *Phys. Rev.* **187** 747–57
[27] Artus M, Ben Tahar L, Herbst F, Smiri L, Villain F, Yaacoub N, Grenèche J M, Ammar S and Fiévet F 2011 Size-dependent magnetic properties of $CoFe_2O_4$ nanoparticles prepared in polyol, submitted
[28] Kodama R H, Berkowitz A E, McNiff J E J and Foner S 1997 Surface spin disorder in ferrite nanoparticles (invited) *J. Appl. Phys.* **81** 5552–7

[29] Kodama R H, Makhlouf S A and Berkowitz A E 1997 Finite size effects in antiferromagnetic NiO nanoparticles *Phys. Rev. Lett.* **79** 1393

[30] Mørup S 2003 Spin-canting and transverse relaxation at surfaces and in the interior of ferrimagnetic particles *J. Magn. Magn. Mater.* **266** 110–8

[31] Anhøj T A, Bilenberg B, Thomsen B, Damsgaard C D, Rasmussen H K, Jacobsen C S, Mygind J and Mørup S 2003 Spin canting and magnetic relaxation phenomena in $Mn_{0.25}Zn_{0.75}Fe_2O_4$ *J. Magn. Magn. Mater.* **260** 115–30

[32] Sawatzky G A, Van Der Woude F and Morrish A H 1968 Cation distributions in octahedral and tetrahedral sites of the ferrimagnetic spinel $CoFe_2O_4$ *J. Appl. Phys.* **39** 1204–5

[33] Kachkachi H, Ezzir A, Nogués M and Tronc E 2000 Surface effects in nanoparticles: application to maghemite γ-Fe_2O_3 *Eur. Phys. J.* B **14** 681–9

[34] Bellitto C, Bauer E M and Righini G 2008 On the crystal structures and magnetism of some hybrid organic–inorganic metal organophosphonates *Inorg. Chim. Acta* **361** 3785–99

[35] Peddis D, Mansilla M V, Mørup S, Cannas C, Musinu A, Piccaluga G, Orazio F, Lucari F and Fiorani D 2008 Spin-canting and magnetic anisotropy in ultrasmall $CoFe_2O_4$ nanoparticles *J. Phys. Chem.* B **112** 8507–13

[36] Aquino R, Depeyrot J, Sousa M H, Tourinho F A, Dubois E and Perzynski R 2005 Magnetization temperature dependence and freezing of surface spins in magnetic fluids based on ferrite nanoparticles *Phys. Rev.* B **72** 184435

[37] De Biasi E, Zysler R D, Ramos C A and Romero H 2002 Magnetization enhancement at low temperature due to surface ordering in Fe–Ni–B amorphous nanoparticles *Physica* B **320** 203–5

[38] Haneda K and Morrish A H 1988 Noncollinear magnetic structure of $CoFe_2O_4$ small particles *J. Appl. Phys.* **63** 4258–60